18TH WORLD CONFERENCE ON EARTHQUAKE ENGINEERING
WCEE2024
MILAN

MILAN, ITALY
30TH JUNE - 5TH JULY 2024

www.wcee2024.it

SAND POST-LIQUEFACTION MONOTONIC RESPONSES WITH VARIOUS LOADING DIRECTIONS AND ANGULARITY

Cesar M. Leal[1], Wing Shun Kwan[2] & Elizabeth R. Nunez[3]

[1]Graduate Research Assistant, California State University, Los Angeles, USA, cleal5@calstatela.edu

[2]Associate Professor, California State University, Los Angeles, USA, wkwan4@calstatela.edu

[3]Graduate Research Assistant, California State University, Los Angeles, USA, enunez54@calstatela.edu

Abstract: *Liquefied sands act like liquid and are dangerous for structures on top of it. It is vital to gain insight into the stress-strain characteristic of liquefied sand, a topic that has not yet been comprehensively explored at the element level. A better knowledge of the materials can improve the engineering assessment of geohazards, such as seismic-induced displacements and settlements. This study investigates liquefied soil by strain-control cyclic loading to induce liquefaction followed by monotonic loading up to a shear strain of 37% in an uni-directional and bi-directional simple shear setup. The testing program in this study focuses on determining the effects of two factors on the post-liquefaction sand response: (1) the effects of loading angles (0, 45, 90, 135, 180, 225, 270, and 315 degrees) between the end of cyclic loading and the start of post-liquefaction monotonic loading, and (2) sand particle roundness. Two types of sand, rounded and angular, were tested at a similar relative density range. The test results show that the loading angles between the pre-liquefaction cyclic and post-liquefaction monotonic loadings have limited effects on the post-liquefaction stress-strain responses. Sand angularity and density provide more impact. The data generated from this study can systemically illustrate the monotonic responses of liquefied sand at eight different angles from its previous phase of cyclic loading and is valuable for calibrations and validations of constitutive models and numerical analyses.*

1. Introduction

Zones with loosely saturated cohesionless soils and high seismic activity are at high risk of liquefaction in the event of an earthquake. Liquefaction is the transformation of saturated cohesionless soils from solid to liquid state due to a rapid dynamic loading resulting in increases in the pore pressure and significant reduction in the strength of the soil (Committee on Soil Dynamics of the Geotechnical Engineering Division 1978). Liquefaction events result in severe damages that affect vital structural components of our modern society, putting lives at risk. The damages include uneven settlement, lateral displacements, bearing capacity failures, and landslides. Significant historical liquefaction events during the 1964 Nigatta and Alaska Earthquakes led the geotechnical engineering community to extensively research soil liquefaction (National Academies of Sciences, Engineering, and Medicine 2021). Despite all the research, an increasing number of investigators agree that crucial areas still need attention, especially understanding the post-liquefaction behaviour of sands, with the majority of the research in the past focusing on soil liquefaction resistance, ground improvement, and understanding pore water generation under undrained conditions (Vaid and Thomas 1995, Kammerer et al. 2002, Sivathayan and Yazdi 2013, Rouholamin et al. 2017). In the past two decades, liquefaction-induced

lateral spreading events in earthquakes like the 1983 Tohoku, Japan, 2011 Christchurch, New Zealand, and 2010 El Mayor Cucapah, Mexico, have been main contributors to the interest in the post-liquefaction behaviour of sands. Considering the post-liquefaction behaviour of sands during the geotechnical design of any structure can result in more earthquake-resilient structures, potentially preventing the negative financial impact from rebuilds needed after liquefaction and, most importantly, saving lives.

The currently available reports from experimental research demonstrated a difference between the pre-liquefaction and post-liquefaction sand stress-strain behaviour. Observations made by Vaid and Thomas (1995) and Sitharam et al. (2009) from triaxial tests have agreed that instantly after liquefaction, close to zero stiffness was maintained with strain increases, then stiffness starts a non-linear climb with increases in strain, then until after some significant deformation, the stiffness and strain increase linearly. These observations are shown in Figure 1(A) as Region 1, Region 2, and Region 3. In recent years, with advances in laboratory equipment, experimental results have provided further understanding of the post-liquefaction stress-strain repose of sands. Investigations by Sivathayalan and Yazdi (2013), Kwan and Huaz (2018), and Mathan et al. (2023) have proposed that under simple shear testing, an additional region can be observed in the post-liquefaction response of sands. As shown in Figure 1 (B) in Region 4, the linear stiffening stops, and a constant strength is reached, which this paper will call post-liquefaction strength (τ_{PL}).

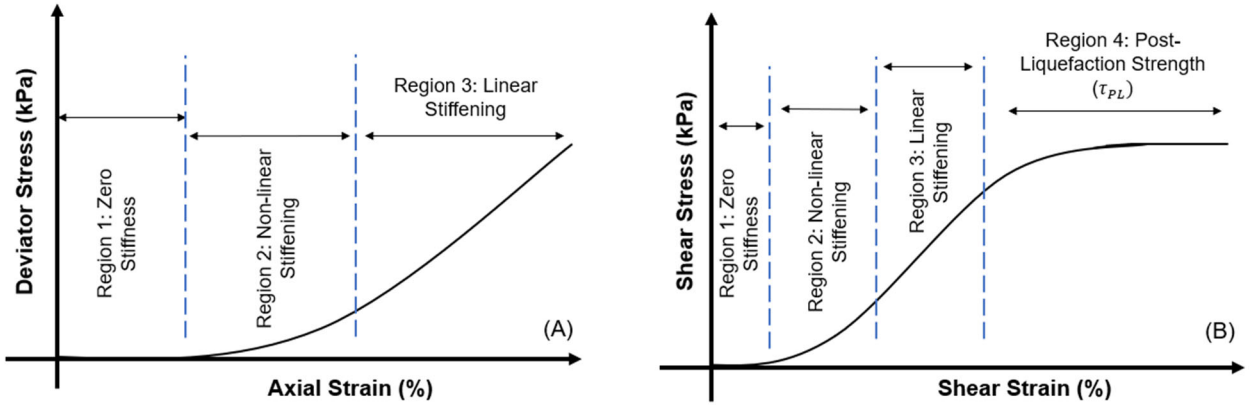

Figure 1. Schematic of Previous Post-Liquefaction Observations (A) Vaid and Thomas (1995) (B) Sivathayalan and Yazdi (2013)

Sivathayalan and Yazdi (2013) concluded that the response after liquefaction is anticipated to be dilative, regardless of the strain history or the nature of the non-liquefied response to loading, but the post-liquefaction strength is governed by loading mode and relative density. With a focus on the effects of relative density (D_R) in the gradual stiffening of liquefied soils, Rounholamin et al. (2017) conducted a series of triaxial tests and found out that as D_R increases, the strain at which the point of transition from Region 1 to Region 2 occurs decreases resulting in very dense sands having significant stiffness right after liquefaction. Kwan et al. (2015) investigated the effects of particle shape on the post-liquefaction response of cohesionless soils under cyclic triaxial testing, respectively, finding that soils composed of well-rounded particles show a brittle response while angular soils show a ductile response. Mathan et al. (2023) recently determined that τ_{PL} increases with particle size and wider gradation. Mele et al. (2023) investigated the response of liquefied soils with post-liquefaction consolidation and concluded that under those conditions, relative density, effective confining stress, CSR, or direction of shear strain (limited to uni-direction) have no significant effect on the post-liquefaction response of sandy soils.

This investigation presents the post-liquefaction behaviour of cohesionless soils under static shear loading with uni-directional and multi-directional simple shear loading modes resulting from 45-degree offset increments from the direction of pre-liquefaction cyclic loading. Post-liquefaction uni-directional simple shear testing has provided key findings in the past years. Nonetheless, these investigations assume that cyclic and post-liquefaction monotonic shear loadings occur in the same direction. However, in reality, soil loading paths can be more complex. First, the direction of pre-liquefaction cyclic loading could be unpredictable because of its random nature. Because of this, it is unlikely that the static shear load experienced by the soil structure right after the seismic loading will be in line with or perfectly perpendicular to the direction of the seismic loading.

Inspired by the randomness in seismic loadings, multi-directional simple shear testing has been widely used in academia to understand the response of soils under cyclic loading (Yang et al. 2016). However, until this date, no record of exploration of these complex loading paths on liquefied soils exists. Therefore, this investigation will provide a further understanding of the post-liquefaction response of soils and the effects of post-liquefaction loading mode and particle angularity by testing in two different soils at eight different loading directions.

Liquefaction initiation occurs in saturated cohesionless soils under undrained conditions. In this study, constant volume simple shear testing was performed, and the equivalency of constant volume settings during cyclic simple shear tests to undrained direct simple shear tests is employed. Dyvik et al. (1987) have investigated and proven that the changes in axial load needed to maintain a constant height during a simple shear test are equivalent to the pore pressure generated during an undrained simple shear test. The marker of liquefaction manifestation during testing varies according to the testing criteria. Some investigators use the double amplitude of 6% in the shear strain to indicate liquefaction. In other studies, excess pore water pressure ratio (r_u) is the liquefaction triggering criteria. For this investigation, the excess pore water pressure ratio (r_u) was adopted as the criteria to define liquefaction in the samples tested. Based on testing results presented by Wu et al. (2004), on average, a r_u value of 0.95 corresponds to 6% double amplitude shear strain criteria, and in dense samples, a r_u value as low as 0.8 can correspond to 6% double amplitude shear strain. Therefore, a r_u value of 0.95 is adopted as the liquefaction triggering criteria for this investigation. After liquefaction was initiated in the soil specimen, we studied the effects of eight different angles between the end of cyclic and post-liquefaction monotonic loadings on two sand types, one relatively rounded and one angular.

2. Testing Program

2.1 Testing Materials

Monterey and Ottawa sand samples were used to conduct multi-stage simple shear testing under constant volume conditions. Ottawa sand is commonly used in research (Salgado 2000, Sivathayan and Yazdi 2013), with predominantly rounded particles. Monterey cohesionless material is characterized by the angularity of its particles and was used in some past liquefaction studies like Kammerer et al. (2002) and Wu et al. (2004). Figure 2 shows the results from the particle size analysis performed according to ASTM D422 for both Ottawa and Monterey Sand used in the testing program. Material properties, including maximum unit (γ_{max}) weight, minimum unit weight (γ_{min}) determined following ASTM standards D4253 and D4254, and classification according to ASTM D2487 Unified Soil Classification System (USCS), are summarized in Table 1.

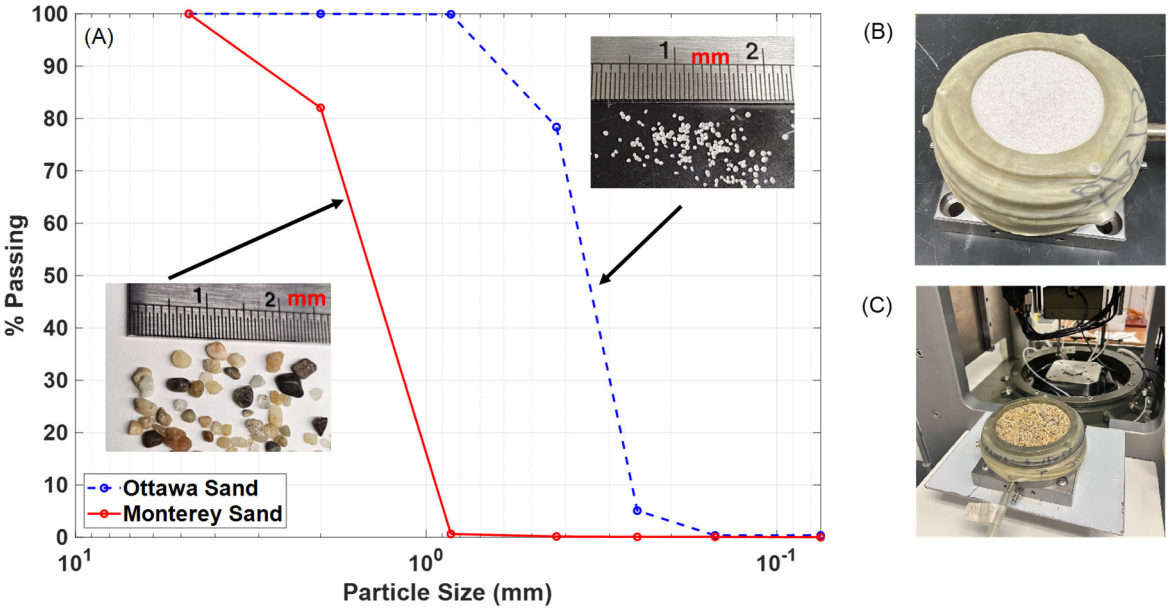

Figure 2. (A) Grain Size Distribution of Ottawa Sand and Monterey Sand (B) Ottawa Sand Sample (C) Monterey Sand Sample

Table 1. Physical Properties of Test Materials

Sand	γ_{min} (kN/m^3)	γ_{max} (kN/m^3)	USCS Classification
Ottawa	14.74	17.22	SP – poorly graded
Monterey	15.29	17.11	SP – poorly graded

2.2 Testing Equipment

The multi-stage simple direct shear testing was performed on a Confined Multi-Directional Dynamic Simple Shear (CMDSS) device at Cal State LA, with two orthogonal horizontal shear actuators (X and Y) (Figure 3A) and the capacity to control each axis individually or simultaneously, the CMDSS device allowed for uni-directional and bi-directional simple shear testing. A six-axis load cell (Figure 3A) aided in measuring and controlling the normal and shear loads experienced by soil samples during testing. The placement of the load cell was as close as possible to the specimen's top to minimize the effects of machine deflection and alignment frictions in the test results. Three Linear Variable Differential Transformers (LVDT) helped measure and control the displacement experience in the X, Y, and Z directions. A critical component was the local LVDT at the Z axis, allowing an accurate measurement of the vertical displacement of the specimens under constant height (volume) cyclic loading. Its placement right at the top cap prevents the introduction of bias from machine deflection in the axial displacement readings.

Sixteen simple shear specimens were reconstituted using 65 mm caps that were securely bolted into the CMDSS device. 1mm thick stacked metal rings provided the confinement needed to maintain a constant diameter. Stacked rings were used to achieve K_o consolidation. In past research, using reinforced membranes allowed for the K_o conditions. However, Kwan and El Mohtar (2014) have shown comparable results between tests performed using reinforced membranes and stacked rings in simple shear testing.

Water tests were necessary to measure and account for any bias in the X and Y axes. During the water test, the 65 mm diameter membrane confined by the metal disks held a water specimen instead of a soil specimen. The Z axis was in touch with the water specimen and set to a constant height to obtain constant volume conditions. The first test goal was to record any bias from machine deflection and friction between stacked metal rings. Liquefied sand behaves like liquid during the "no-stiffness" phase, so correcting any frictional bias from the testing apparatus is important. The X-axis was set to travel up to 37% shear strain at a shear rate of 1mm per 80 minutes. The second test aimed to measure any bias from friction between stacked rings in a bi-directional simple shear setup. The settings for the second test consisted of the X and Y axes set to displace simultaneously (i.e., 45 degrees) until 37% shear strain was reached. Figure 3B presents the results from the water tests performed at loading directions of 0 and 45 degrees. The results from these water tests show similar stress-strain responses with minor frictional effects, indicating that the results presented later in the text have a minimal bias of less than 0.5 kPa at 25% shear strain in either uni-directional or bi-directional loading paths. All the results presented in this paper were corrected as a function of the shear strain.

2.3.1 Sample Preparation

A total of 16 simple shear tests were conducted from clean Monterey and Ottawa sand. All samples were reconstituted using the dry pluviation method (Kwan and El Mohtar 2020) to a nominal 65 mm diameter and an average 22 mm height. With the goal of triggering liquefaction during the dynamic loading stage in medium-dense samples, all samples were maintained between 40 and 50 percent density relative to Ottawa and Monterey sand maximum and minimum densities, respectively. Table 2 shows a summary of the tests performed. The Dr_i presented refers to the relative density of the pre-consolidated sample, and Dr_f refers to the relative density of the specimen post-consolidation right before cyclic loading was initiated. Further explanation of the results presented in Table 2, cycles to failure (N_{r_u}), post-liquefaction strength (τ_{PL}), and post-dilation strain (γ_{PD}) is provided in the results section.

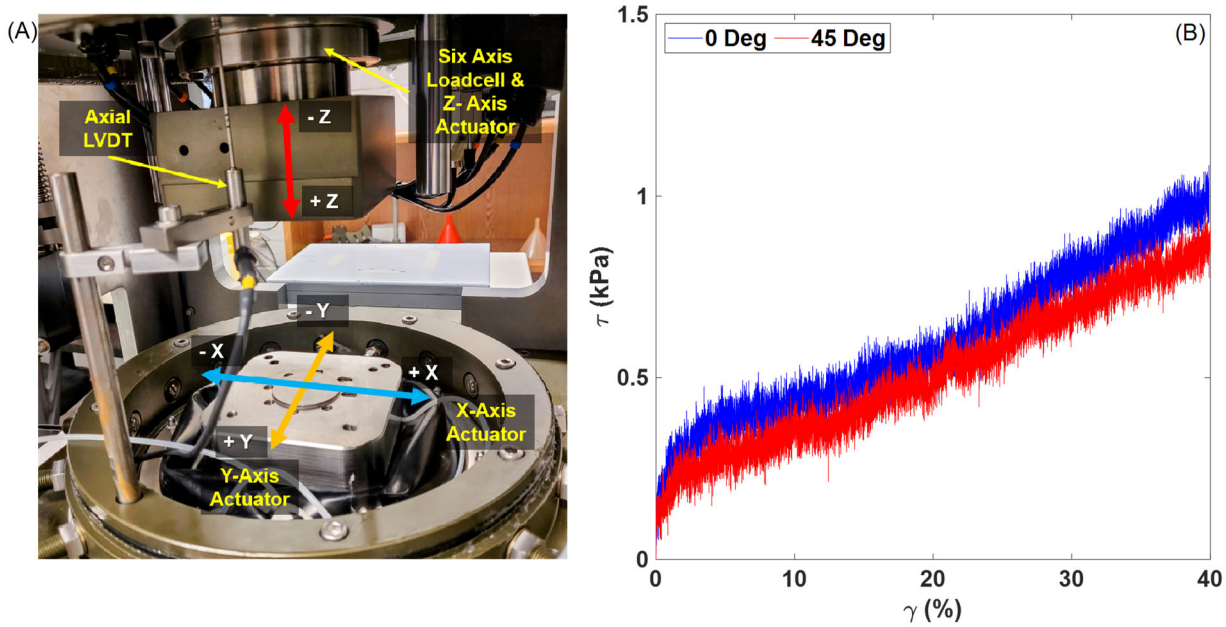

Figure 3 (A) CMDSS Three-axis Actuation and Instrumentation; (B) 0 degree and 45 degrees Water Test Results

Table 2. Multi-Stages and Bi-Directional Cyclic Simple Shear Test Summary

ID #	Sand Type	D_{ri} (%)	D_{rf} (%)	Post-Liq Rotation (°)	$N_{r\_u=0.95}$	$N_{r\_u=0.90}$	τ_{PL} (kPa)	γ_{PD} (%)
1	Monterey	45.3	47.5	0	3.39	2.40	456.66	6.5
2	Monterey	38.3	41.9	45	1.94	1.36	410.55	7.9
3	Monterey	44.1	46.1	90	5.39	3.37	558.87	8.6
4	Monterey	32.9	36.9	135	2.37	1.86	296.40	8.2
5	Monterey	46.7	50.9	180	3.37	2.39	540.66	6.9
6	Monterey	43.5	47.9	225	2.37	1.91	523.76	6.7
7	Monterey	40.7	42.7	270	2.46	1.88	400.28	7.8
8	Monterey	43.0	45.0	315	1.89	1.42	487.04	7.4
9	Ottawa	48.4	52.7	0	3.94	2.37	122.02	3.3
10	Ottawa	47.6	51.3	45	7.43	3.91	81.95	~ 0
11	Ottawa	41.7	46.5	90	5.46	3.89	76.59	~ 0
12	Ottawa	43.8	49.9	135	5.39	3.93	116.20	~ 0
13	Ottawa	43.9	52.9	180	5.88	3.87	86.67	~ 0
14	Ottawa	50.2	56.7	225	7.45	5.44	98.26	~ 0
15	Ottawa	43.2	50.2	270	4.91	3.89	69.23	~ 0
16	Ottawa	43.3	47.8	315	4.43	2.91	86.96	~ 0

2.3.2 Consolidation and Cyclic Testing

The testing schedule was divided into three stages: 1) Consolidation, 2) 10-cycle cyclic strain loading, and 3) Post-liquefaction monotonic loading (Figure 4). Each soil sample was consolidated to a vertical stress of 100

kPa while tracking the axial displacement with the local Z-axis LVDT. The testing proceeded to the second stage after observing no further axial displacement at the targeted vertical stress. The second stage involved constant volume cyclic simple shear following ASTM D8296. Strain control was employed to achieve the dynamic loading to generate shear stresses in the specimen, a sinusoidal displacement in the X-axis equivalent to a single amplitude (SA) displacement equal to one percent of the post-consolidation height of each sample. Strain control was chosen over stress control in an attempt to achieve a relatively consistent dissipation of energy during cyclic loading in every test. Furthermore, by controlling the horizontal actuator using displacement, every test ended the cyclic phase at the zero position, allowing an accurate reference for all post-liquefaction monotonic tests. Expecting liquefaction initiation to occur within ten cycles under the loading of 1% SA shear strain, each specimen underwent a total of ten dynamic loading cycles, intending to introduce a relatively equal amount of dissipated energy in stage 2 before entering the next stage of post-liquefaction monotonic loading. The results showed that a r_u = 0.95 is achieved around five cycles for Ottawa sand and 2.8 cycles for Monterey sand tests. In order to fix the volume of the soil sample during cyclic loading, the Z-axis actuator was commanded to maintain the sample post-consolidation height throughout the pre-liquefaction cyclic and post-liquefaction monotonic stages. We investigated the effects of loading angles in liquefied sand without the consideration of re-consolidation between the pre-and post-liquefaction stages.

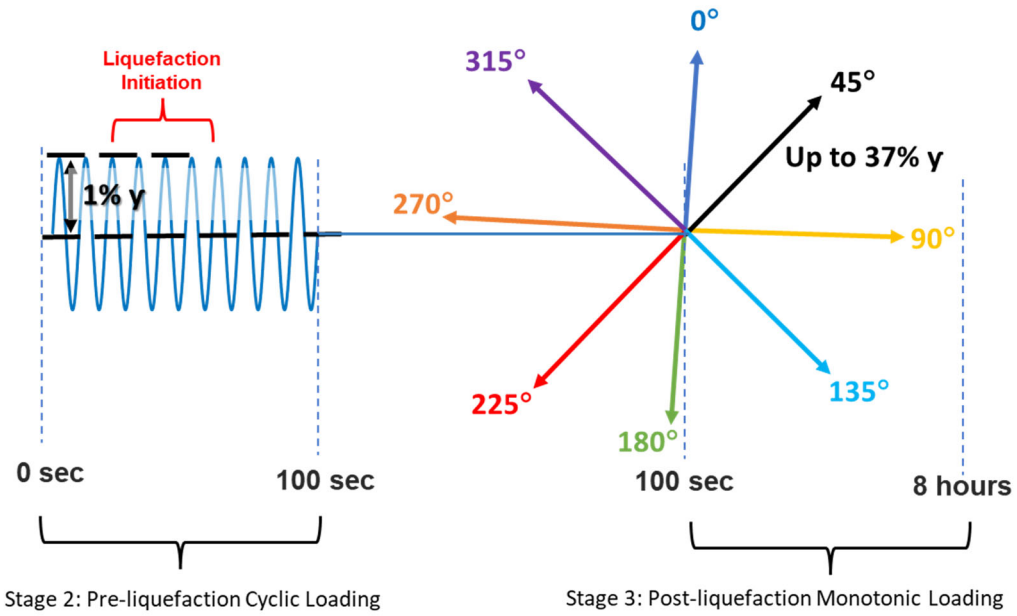

Figure 4. Strain Path for Multi-Stage Test Plan

2.3.3 Post-Liquefaction Monotonic Test (Post-Mono)

The third stage was initiated after the manifestation of liquefaction and the completion of all ten dynamic loading cycles. The third stage involved monotonic simple shear testing at different directions from the endpoint of the cyclic stage. Eight tests were performed for each Ottawa sand and Monterey sand. The first test was set to continue on the dynamic loading path (0 degrees) on the positive X-axis. As shown in Figure 4, the subsequent tests were set at 45-degree increments from the positive X-axis. Tests at 45, 135, 225, and 315 degrees were conducted with the combination of X and Y-axis actuators to displace in a bi-directional setup. For the uni-directional monotonic tests (0, 90, 180, and 270 degrees), the X-axis (0 and 180 degrees) or Y-axis (90 and 270 degrees) shifted from 0 to 37% shear strain while the other was fixed. For bidirectional monotonic tests (45, 135, 225, and 315 degrees), the X and Y axes were commanded to displace up to 37% shear strain simultaneously at a shear rate of 1 mm per 80 min (Lacasse and Berre 1988) in all directions. The travel path can be thought of as a resultant displacement with X and Y components forming a right triangle, and by the Pythagorean Theorem, the resultant displacement and stress are the square root of the sum of square X and Y displacements and stresses. The general settings for each monotonic test included the Z-axis actuator under displacement control fixed at the post-cyclic height of the specimen and the X and Y-axis actuators under displacement control.

3. Test Results and Discussion

3.1 Cyclic Test

The results of the 16 simple shear tests are divided into two sets. The first set presents the cyclic (second stage) phase results in Figure 5. Figure 5A presents the pore pressure generation in terms of the pore pressure ratio (r_u). A consistent pore pressure generation during cyclic loading can be observed in all Monterey sand samples, indicating a similarity in the sample fabric before cyclic loading. Figure 5B shows that the same applies to all the tested Ottawa sand specimens. Overall, the peak pore pressure ratios range from 0.95 to 1 in all specimens, indicating the manifestation of liquefaction in all sand samples tested by the criteria adopted for this investigation. Previously, in Table 2, the cycles to failure ($N_{r\_u=0.95}$ and $N_{r\_u=0.9}$) were presented. These values emerge from counting the number of cycles (N) needed for each specimen to reach a pore pressure ratio (r_u) equal to 0.95 or 0.9, translating to the failure of the specimen with axial stress getting very close to zero. $N_{r\_u=0.95}$ values reflect that, on average, Ottawa sand tests (average $D_{rf=}$ = 45.3 %) presented more resistance to liquefaction, with an average of 5.6 cycles. With an average of $N_{r\_u=0.95}$ = 2.9 cycles, Monterey sand tests (average D_{rf}= 41.8 %) showed minor resistance to liquefaction compared to Ottawa sand specimens. The comparison of the $N_{r\_u=0.95}$ values to post-consolidation relative density (Figure 5C) shows that as D_{rf} increases, the number of cycles to liquefaction also increases. Figure 5D shows examples of stress path, and Figure 5E shows examples of stress-strain curves.

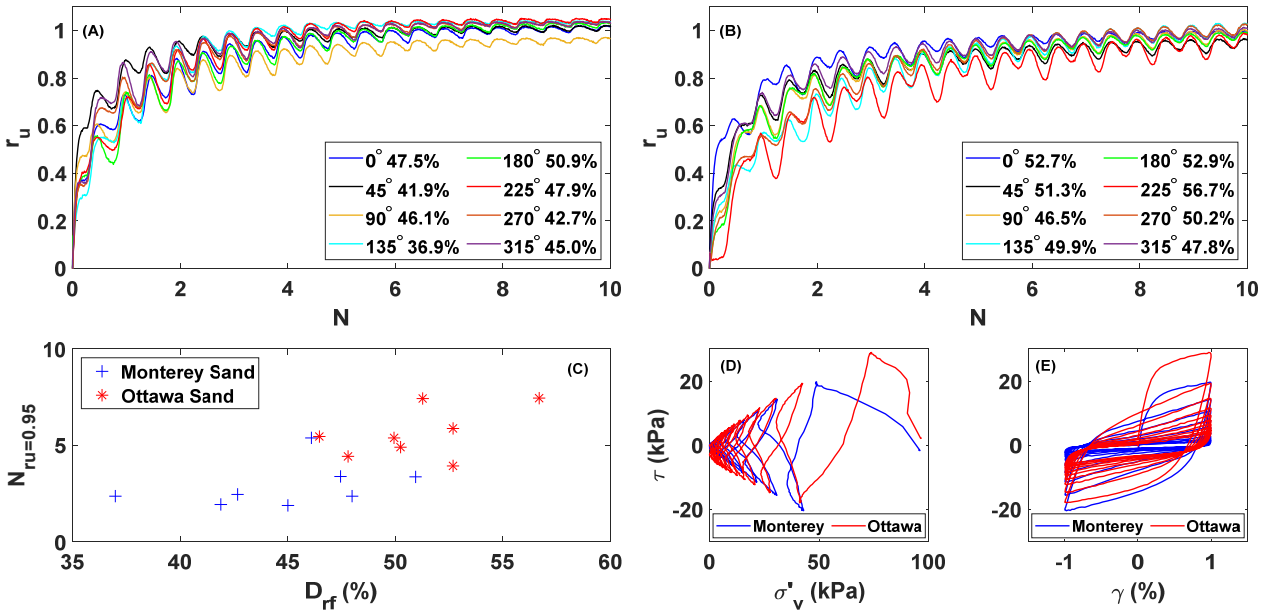

Figure 5 (A) Pore Pressure Generation in Monterey Specimens (legends show loading degrees between the pre-cyclic and post-monotonic stages and relative densities in %), (B) Pore Pressure Generation in Ottawa Sand Specimens (C) Post-Consolidation Relative Density vs. Cycles to Liquefaction (D) Stress Paths (Test #3 & #11); and (E) Stress-Strain (Test #3 & #11)

3.2 Post-Liquefaction Monotonic Test

The post-liquefaction monotonic simple shear testing results from Monterey and Ottawa sand specimens, shown in Figure 6, follow the expected dilative pattern described at the introduction with a low-stiffness region that transitions into the stiffening regions until reaching the peak post-liquefaction strength. The post-liquefaction strength (τ_{PL}) reached by specimens made with Monterey sand ranges from 200 kPa to near 600 kPa with an average of 459 kPa and a standard deviation of 87.72 kPa. Ottawa specimens showed a lower post-liquefaction strength with an average of 92 kPa and 18.66 kPa standard deviation. As shown in Figures 6A and 6B, the post-liquefaction strength increases randomly with the direction of static loading. For example, in Monterey tests, the τ_{PL} decreases for test #2 (45 deg.) when compared with test #1 (0 deg.), but then it increases for test #3 (90 deg.). The post-liquefaction strength against the post-consolidation relative density of the samples is presented in Figures 6C and 6D, revealing a correlation with the relative density. These results align with the findings from Sivathayalan et al. (2013). The experimental data shows that post-

liquefaction strength increases as the post-consolidation relative density (Dr_f) increases. This relationship appears to be stronger with the Monterey Sand (R^2 = 0.80) than with the Ottawa Sand (R^2 = 0.13).

Further observations can be made when comparing the post-liquefaction strength from the Monterey and Ottawa sand tests. The average post-consolidation relative density of Monterey samples was 41.82 percent, with a standard deviation of 4.46 percent. In the same manner, the average post-consolidation relative density of Ottawa specimens was determined to be 45.25 percent with a 3.02 percent standard deviation. A lower dispersion in the Ottawa results exists. These results, combined with the spreading of the post-liquefaction strength gained by the samples, indicate that Ottawa sand specimens (rounded material) experience minor changes in post-liquefaction shear strength with fluctuations in relative density compared with Monterey sand samples (angular material) displaying variations in the post-liquefaction shear strength with a larger magnitude, with similar fluctuations in relative density. As shown in Figures 6C and 6D, a simple linear mathematical model of the correlation between relative density and post-liquefaction strength indicates that the correlation between post-liquefaction strength and post-consolidation relative density is weak in rounded materials (R^2 = 0.13), but relatively stronger in the more angular materials (R^2 = 0.80).

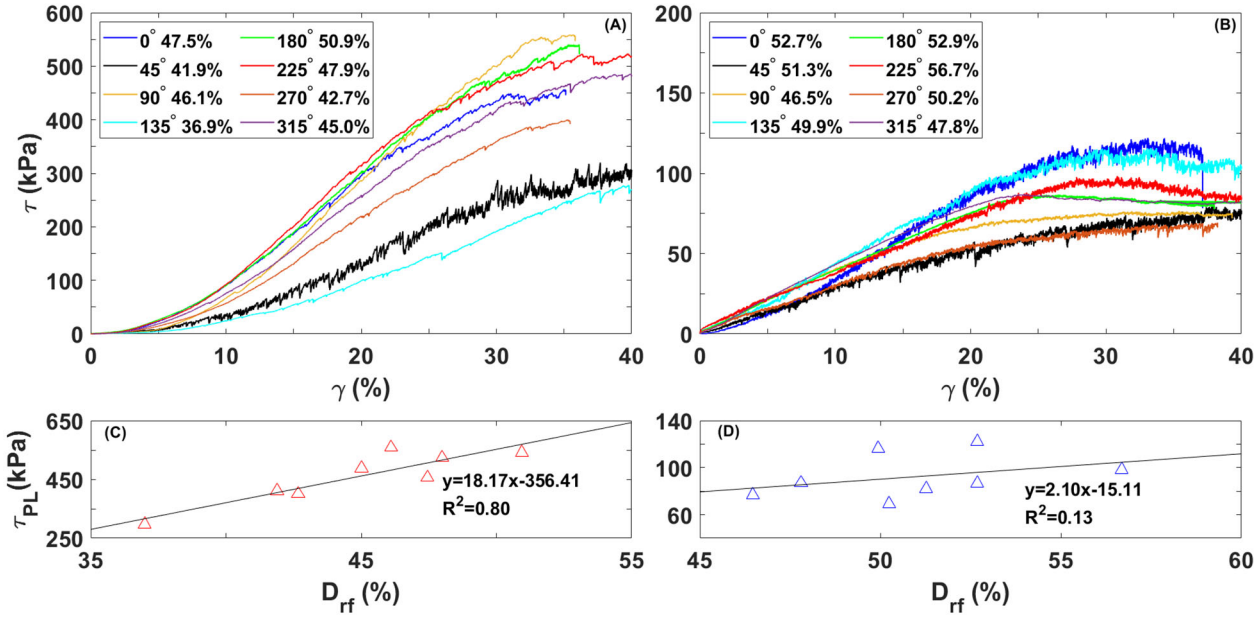

Figure 6 – (A) Monterey Post-Liquefaction Monotonic Stress vs. Strain; (B) Ottawa Post-Liquefaction Monotonic Stress vs Strain; (C) Monterey Max Post-Liquefaction Strength vs. D_{rf}; (D) Ottawa Max Post-Liquefaction Strength vs. D_{rf}

Another behaviour observed is the magnitude of the shear strain needed to reach the post-liquefaction strength region in the dilative stress-strain response. For discussion, this paper will refer to this magnitude as post-liquefaction strain (γ_{PL}). Figures 6A and 6B show that the liquefied specimens made with Ottawa sand, on average, reached a post-liquefaction strength after approximately 27% post-liquefaction strain. On the other hand, samples made with more angular material displaced more than 35% post-liquefaction strain on average before reaching the post-liquefaction strength. This behaviour agrees with observations by Kwan et al. (2015), with angular materials having a ductile post-liquefaction response and rounded materials having a more brittle response. These observations indicate that angularity does affect the post-liquefaction stress-strain response of medium-dense sands.

There is a no-stiffness region in a typical post-liquefaction stress-strain response that can be described by the post-dilation strain (γ_{PD}), and Figure 7A depicts the terms of τ_{PL}, γ_{PD}, and γ_{PL} on the stress-strain curve of Test #1. From the outcome of our testing program, it can be observed that Ottawa sand specimens had a relatively small no-stiffness region, with stiffing happening almost right after liquefaction (Figure 7C). In contrast, Monterey samples experienced a larger significant displacement before stiffening (Figure 7B). The almost instantaneous stiffening of Ottawa sand is the main contributor to the minor post-liquefaction strain. Rounholamin et al. (2017) investigated the strain magnitude at the transition between the stiffening region,

which for this paper will be referenced as post-dilation strain (γ_{PD}). They concluded that it depended on the post-consolidation relative density, with dense samples stiffening almost immediately after liquefaction.

Rounholamin et al. (2017) proposed modeling the stress-strain response of liquefied soils, previously shown in Figure 1, as a bi-linear curve with a lower rate of change in Region 1 than the linear stiffening region. Using this concept, as shown in Figure 7A, a best-fit line through the no-stiffness region (Region 1) and a second-best-fit line through the steepest region (Region 3) were used to determine the dilative strain parameter, γ_{PD}. The slope of these lines is referenced as the initial shear modulus and the critical state shear modulus, respectively. The application of the bi-linear model was successful in all Monterey sand. Figure 7B shows a closeout view of the post-liquefaction stress-strain response of all Monterey sand samples, and an evident change in slope takes place in all tests. From this analysis, it can be established that, on average, it takes 7 percent of the total displacement for the transition point to occur on Monterey specimens. On the other hand, as shown in Figure 7C, on Ottawa specimens, only test #9 ($\theta = 0^o$) shows an evident slope change. For the rest of the tests, an instantaneous stiffening is observed to start at very small strain levels. Post-dilation strain (γ_{PD}) was assumed to be zero for these tests. We investigated the relationships between the post-dilation strain and relative density from the results obtained, and there is no apparent correlation ($R^2 < 0.1$) between the two parameters.

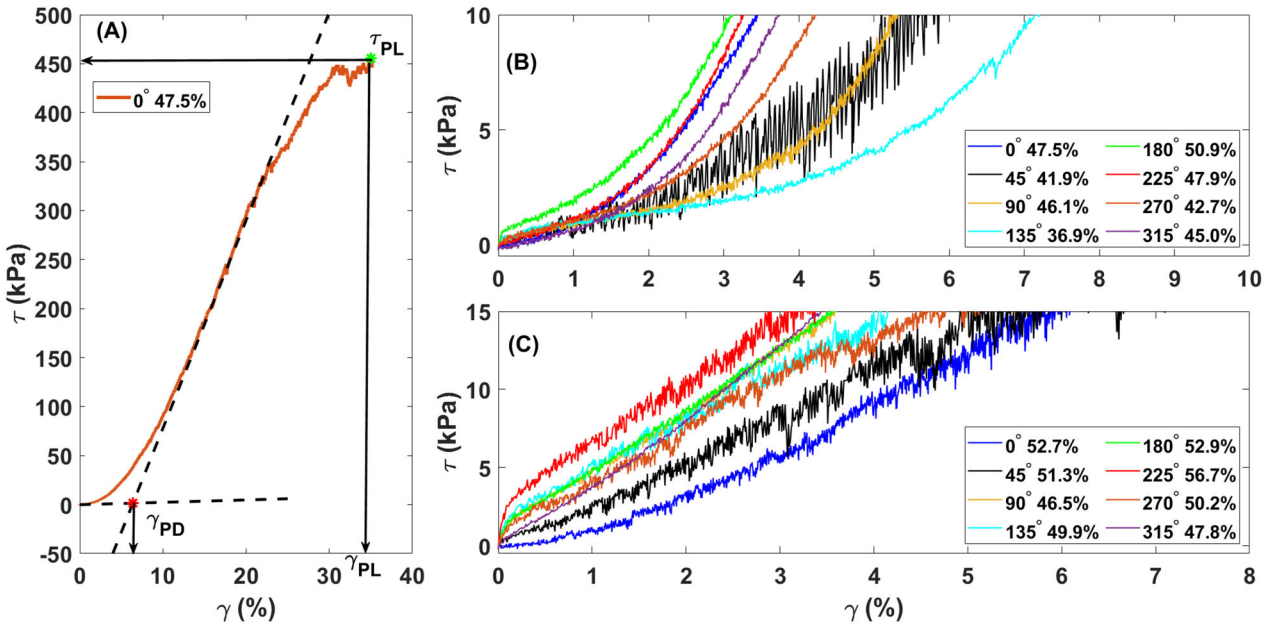

Figure 7 (A) Rounholamin et al. (2017) Bi-linear curve modeling for γ_{PD}, and demonstrations of τ_{PL} and γ_{PL}; (B) Initial Portion of Monterey Sand Post-Liquefaction Responses; (C) Initial Portion of Ottawa Sand Post-Liquefaction Responses

Figure 8 summarizes the values of post-liquefaction shear strength (τ_{PL}) and post-liquefaction dilation strain (γ_{PD}) from the sixteen test results, along with the relative density of each test. Ranking from the highest to the lowest for the two parameters is also provided, except for the Ottawa sand γ_{PD} values (all but one is zero). These results exhibit no clear relationship between the post-liquefaction strength and the direction of static loading, except there may be an indication of weaker post-liquefaction strength when the loading angle between pre-cyclic and post-monotonic is 270 degrees. The lowest post-liquefaction strength (8th rank) was recorded in Ottawa sand, and the second weakest strength (7th rank) was recorded in Monterey sand. However, further tests on a different type of sand will be needed to confirm this observation. Figure 9 shows the comparisons between post-liquefaction strength and loading angles; no clear correlation or pattern exists.

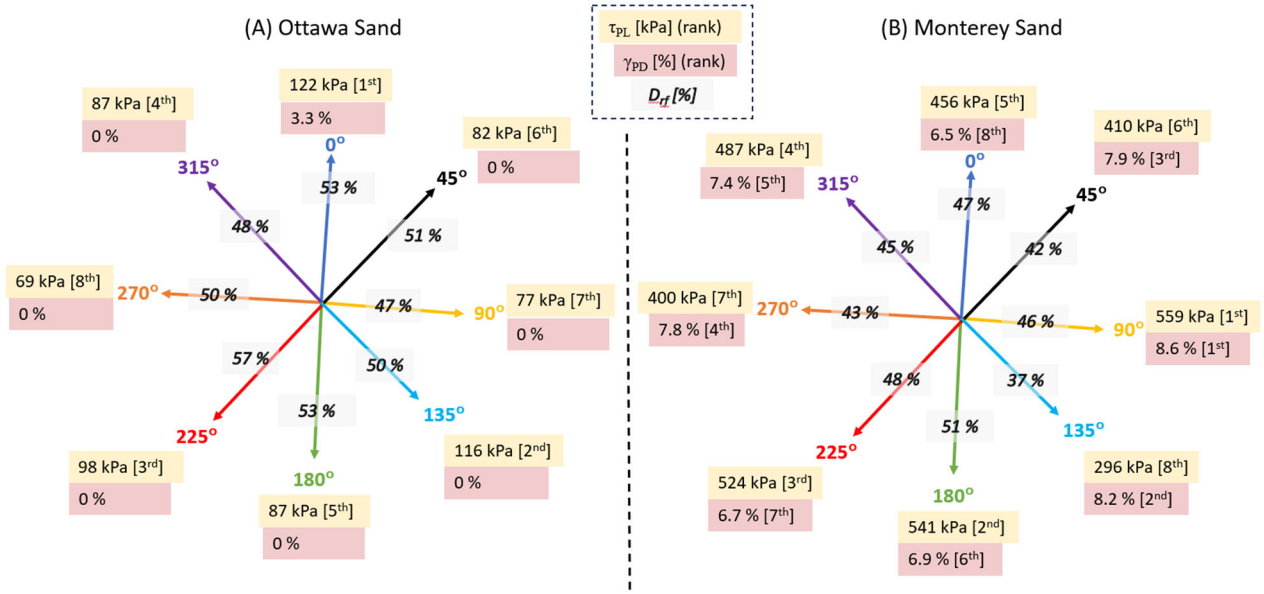

Figure 8 – Summaries of Post-Liquefaction Responses from the 16 tests. Legends indicate (1) post-liquefaction monotonic maximum shear strength, τ_{PL}, highlighted in yellow, (2) post-liquefaction transitional shear strain, γ_{PD}, highlighted in red, and (3) relative density, D_{rf}, highlighted in gray. Ranking provided for τ_{PL} and γ_{PD} from highest to lowest.

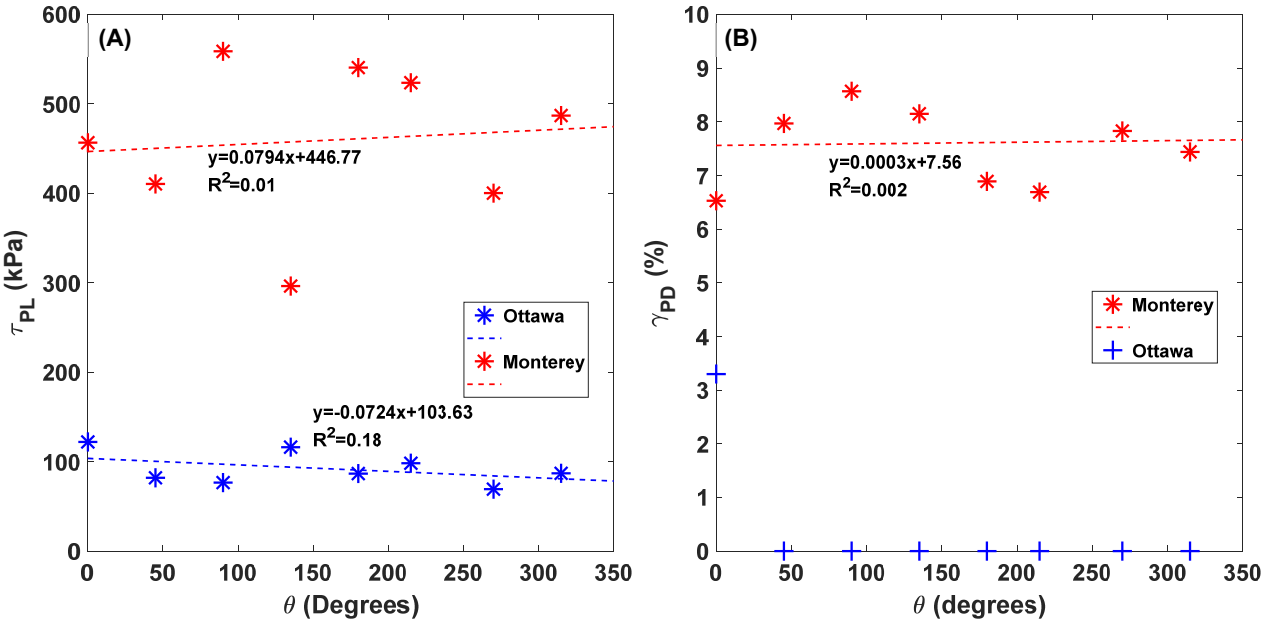

Figure 9 (A) Comparison between the post-liquefaction strength (τ_{PL}) and loading angle between the pre-liquefaction cyclic stage and post-liquefaction monotonic stage; (B) Comparison between post-liquefaction dilation strain γ_{PD} and loading angle between the pre-liquefaction cyclic stage and post-liquefaction monotonic stage

4. Conclusion

To study the post-liquefaction behaviour of cohesionless soils, specimens that experienced liquefaction initiation were subject to a monotonic loading at different loading angles (directions) using a bi-directional simple shear device. Two types of sand, one rounded (Ottawa sand) and one angular (Monterey sand), were utilized to investigate the effects of particle shapes. The post-liquefaction behaviour of cohesionless soils can be affected by angularity and relative density. The post-liquefaction test results from this investigation show limited effects from the direction of loading on the post-liquefaction shear strength. A loading angle of 270

degrees between the pre-liquefaction cyclic and post-liquefaction monotonic loadings appears to provide lower post-liquefaction strengths. As particle angularity increases, the peak post-liquefaction shear strength appears to have a stronger dependency on pre-liquefaction relative density. The post-dilation strain appears to increase as particle angularity increases, with the Ottawa sand test recovering stiffness almost immediately after liquefaction and the Monterey test, on average, requiring 7% strain for significant stiffening to occur. Also, the results show that post-dilation strain is not affected by minor dispersions in the post-consolidation relative density. Overall, the recovery strain is generally higher in the Monterey sand tests, with more displacement needed to gain shear strength as angularity increases.

5. Acknowledgment

The acquisition of the Confined Multi-Directional Dynamic Simple Shear device was supported by the National Science Foundation with Award No. 2117908. Cesar Leal and Elizabeth Nunez are recipients of the CREST-CATSUS fellowship, for which we are grateful. This work has also been partially supported by the National Science Foundation with Award No. HRD-2112554 and Cal State LA Gunjit S. Sikand Faculty Research Fellowship. These supports are gratefully acknowledged.

6. References

ASTM D422-07. *Standard Test Method for Particle-Size Analysis of Soils. ASTM International, West Conshohocken*, PA, www.astm.org

ASTM D2487-17. *Standard Practice for Classification of Soils for Engineering Purposes (Unified Soil Classification System)*. ASTM International, West Conshohocken, PA, www.astm.org

ASTM D4253-16. *Standard Test Methods for Maximum Index Density and Unit Weight of Soils Using a Vibratory Table*. ASTM International, West Conshohocken, PA, www.astm.org

ASTM D4254-16. *Standard Test Methods for Minimum Index Density and Unit Weight of Soils and Calculation of Relative Density*. ASTM International, West Conshohocken, PA, www.astm.org

ASTM D8296-19. *Standard Test Method for Consolidated Undrained Cyclic Direct Simple Shear Test under Constant Volume with Load Control or Displacement Control*. ASTM International, West Conshohocken, PA, www.astm.org

Committee on Soil Dynamics of the Geotechnical Engineering Division (1978). "Definition of terms related to liquefaction." *Journal of Geotechnical Engineering Division*. 104 (9), 1197–1200.

Dyvik R., Berre T., Lacasse S., Raadim B. (1987). Comparison of truly undrained and constant volume direct simple shear tests. *Géotechnique*. 37 (1). 3–10.

Mele L., Lirer S., Flora A. (2023). "Experimental investigation on the post-liquefaction behavior of sands in simple shear conditions." *Geotechnical Testing Journal*. 46 (6). 1–24.

Kammerer, A. M., Pestana J. M., Seed R. B. (2002). Undrained response of Monterey 0/30 sand under multi-directional cyclic simple shear loading conditions. Ph.D. Dissertation, UC Berkeley.

Kwan, W. S., El Mohtar, C. S. (2020). "A review on sand sample reconstitution methods and procedures for undrained simple shear test." *International Journal of Geotechnical Engineering*, 14(8), 851–859.

Kwan, W. S., El Mohtar, C. S. (2014). Comparison between Shear Strength of Dry Sand Measured in CSS Device Using Wire-Reinforced Membranes and Stacked Rings, *ASCE Geo-Congress*. 1111–1119.

Kwan, W.S., Huaz, J. (2018). Effects of irregular loading on sand responses before and after liquefaction initiation, *11th U.S National Conference on Earthquake Engineering*, Los Angeles, California.

Kwan, W.S, Nichols, A., El Mohtar, C. (2015). 'The effect of irregular preliquefaction loading and particle angularity on postliquefaction response', *Proceedings of the 10th Pacific Conference on Earthquake Engineering: Building an Earthquake-Resilient Pacific*, Sydney, Australia.

Lacasse, S., Berre, T. (1988). Triaxial testing methods for soils. Advanced Triaxial Testing of Soil and Rock, *ASTM STP977*, 264–389.

Manmatharajan M. V., Ingabire E., Sy A., Ghafghazi M. (2023). Effect of particle size and particle size distribution on the post-liquefaction strength of granular soils. *Soils and Foundations*. 63 (4).

National Academies of Sciences, Engineering, and Medicine. (2021). State of the Art and Practice in the Assessment of Earthquake-Induced Soil Liquefaction and Its Consequences. *Washington, DC: The National Academies Press*. https://doi.org/10.17226/23474.

Rouholamin M., Bhattacharya S., Orense R. P. (2017). Effect of initial relative density on the post-liquefaction behaviour of sand. *Soil Dynamics and Earthquake Engineering*. 9725–36.

Salgado R. Bandini P., Karim A., (2000) “Shear Strength and Stiffness of Silty Sand.” *Journal of Geotechnical and Geoenvironmental Engineering*. 126 (5), 451–462.

Sitharam T. G., Vinod J. S., Ravishankar B. V. (2009). Post-liquefaction undrained monotonic behaviour of sands: experiments and DEM simulations. *Géotechnique*. 59 (9), 739–749.

Sivathayalan S., Yazdi, A. M. (2014). Influence of strain history on postliquefaction deformation characteristics of sands. *Journal of Geotechnical and Geoenvironmental Engineering*. 140 (3).

Vaid Y. P., Thomas, J. (1995). Liquefaction and postliquefaction behavior of sand. *Journal of Geotechnical Engineering*. 121 (2), 163–173.

Wu J., Kammerer A. M., Riemer M.F., Seed R.B., Pestana J. M. (2004). ‘Laboratory study of liquefaction triggering criteria’, *Proceedings of the 13th World Conference on Earthquake Engineering Conference*, Vancouver, Canada.

Yang M., Taiebat M., Vaid Y. (2016). Bidirectional monotonic and cyclic shear testing of soils: state of knowledge, *69th Canadian Geotechnical Conference*, Vancouver, Canada.